Surface Expression of Low Basal Friction Upstream of Antarctic Grounding Lines

Journal:	*Annals of Glaciology*
Manuscript ID	Draft
Manuscript Type:	Article
Date Submitted by the Author:	n/a
Complete List of Authors:	Stewart, Ella; Georgia Tech, Earth and Atmospheric Sciences Robel, Alexander; Georgia Tech, Earth and Atmospheric Sciences Chu, Wing (Winnie); Georgia Tech, School of Earth and Atmospheric Sciences
Keywords:	Antarctic glaciology, Subglacial processes, Remote sensing, Ice shelves
Abstract:	Ice sheets leave contact with the bed at grounding lines, beyond which floating ice shelves experience no friction at their base. In places where basal friction begins to decrease upstream of the grounding line, ice sheets respond more strongly to climate forcing. However, the spatial extent of zones of low grounding line friction is poorly constrained by observations. Here, we use a steady-state model of marine-terminating ice stream flow to show that the location where basal friction begins to weaken upstream of the grounding line is accompanied by a prominent surface slope break. We then use observations of grounding zone features around the Antarctic Ice Sheet derived from ICESat-2 laser altimetry to find the displacement between grounding line locations determined from SAR flexure measurements and such surface slope break points. We find widespread evidence of decreasing friction hundreds to thousands of meters upstream of grounding lines around the Antarctic Ice Sheet, indicating that grounding lines may be more sensitive to forcing than typically assumed in ice sheet models where friction does not decrease upstream of the grounding line. We suggest that such an observational approach should be used to parameterize grounding line friction interpolation schemes in ice sheet models.

Surface Expression of Low Basal Friction Upstream of Antarctic Grounding Lines

Ella STEWART,[1] Alexander A. ROBEL,[1] Winnie CHU,[1]

[1] *School of Earth and Atmospheric Sciences, Georgia Institute of Technology*

Correspondence: Alexander A. Robel <robel@eas.gatech.edu>

ABSTRACT. Ice sheets leave contact with the bed at grounding lines, beyond which floating ice shelves experience no friction at their base. In places where basal friction begins to decrease upstream of the grounding line, ice sheets respond more strongly to climate forcing. However, the spatial extent of zones of low grounding line friction is poorly constrained by observations. Here, we use a steady-state model of marine-terminating ice stream flow to show that the location where basal friction begins to weaken upstream of the grounding line is accompanied by a prominent surface slope break. We then use observations of grounding zone features around the Antarctic Ice Sheet derived from ICESat-2 laser altimetry to find the displacement between grounding line locations determined from SAR flexure measurements and such surface slope break points. We find widespread evidence of decreasing friction hundreds to thousands of meters upstream of grounding lines around the Antarctic Ice Sheet, indicating that grounding lines may be more sensitive to forcing than typically assumed in ice sheet models where friction does not decrease upstream of the grounding line. We suggest that such an observational approach should be used to parameterize grounding line friction interpolation schemes in ice sheet models.

INTRODUCTION

The grounding line is a critical junction where flowing glacier ice transitions form being in contact with the solid earth to floating on seawater. Friction at the base of ice sheets, especially near the grounding line, is a critical factor for ice flow dynamics and marine ice sheet stability. Decreased basal friction near the grounding line increases ice flow velocity through the grounding line and may lead to increased ice sheet sensitivity to climate forcing and more rapid retreat following grounding line destabilization (Tsai and others, 2015; Brondex and others, 2017; Zhao and others, 2025). Basal friction is influenced by conditions such as bed roughness, till deformation, subglacial hydrology, and seawater intrusion under grounded ice. The intrusion of warm seawater under grounded ice, in particular, can accelerate ice flow through simultaneously lubricating the bed and increasing basal ice melt. Previous theory, experiments, and observations have found that it is physically plausible for a layer of dense seawater to penetrate many kilometers inland from the terminus over a flat or reverse sloped impermeable bed (Wilson and others, 2020; Robel and others, 2022b; Gadi and others, 2023; Rignot and others, 2024). Simulations with large-scale ice sheet models have found that basal melt from seawater intrusion may substantially increase ice loss projections (Seroussi and others, 2019; Robel and others, 2022b). While models can include low basal friction upstream of the grounding line with sub-element parameterizations (Seroussi and others, 2014), there is a lack of observations to constrain whether such low-friction basal regimes do in fact exist near real grounding lines.

Tsai and others (2015) investigated the effect of including a transition to Coulomb basal sliding near the grounding line of a marine ice sheet model, while retaining power-law sliding upstream. This is distinct from the form of basal sliding typically used in marine ice sheet modeling (e.g., Schoof, 2007, and most modern ice sheet models) where basal friction is set by power-law sliding everywhere, and so is high right up to the grounding line, where it goes to zero instantaneously in space. In contrast, the consideration of Coulomb sliding imposes a constant basal stress which drops gradually to zero as the ice loses contact with the bed near the grounding line. Tsai and others (2015) find that transitioning from a power-law to a Coulomb regime, where the basal shear stress approaches zero near the grounding line, leads to a distinct surface slope profile. They note that, "whereas the ice-sheet surface is steepest at the grounding line under power-law drag, with Coulomb friction it tapers off toward the grounding line." Though the implication of this finding is not discussed further by the authors, this result indicates that the surface slope expression of low basal friction near the grounding line is distinct from the surface expression with an step-like loss of basal friction at the grounding line, and may provide a useful means of identifying such a difference in observations.

Subglacial conditions are logistically challenging to measure in situ under thick polar ice sheets. Ice surface observations, however, are now more accessible than ever due to the proliferation of satellite missions measuring various surface properties of ice sheet. The Ice, Cloud, and Land Elevation Satellite-2 (ICESat-2) mission, launched by NASA in 2018, is one such mission which measures ice sheet surface elevation at unprecedented accuracy and horizontal resolution. The purpose of this work is to investigate the potential utility of ice surface observations for detecting low-friction basal regimes near grounding lines. We approach this problem first by modeling the surface expression of low-friction basal regimes and hypothesizing that decreasing basal friction upstream of the grounding line produces a unique surface slope change that is sufficiently large so as to be detectable in satellite altimetry and distinct from other possible spatial variations in basal properties. We then analyze an existing dataset of grounding line surface features in Antarctica derived from satellite altimetry. We find widespread evidence for low basal friction upstream of Antarctic grounding lines, and conclude by highlighting the implications for modeling low-friction basal regimes.

HYPOTHESIS FROM MODELING

We use a 1D depth-integrated flowline model of a marine-terminating glacier with an unconfined ice shelf to understand how changes in basal friction near the grounding line are manifested in the ice sheet surface geometry observable by satellites. In this study, we only consider the steady-state solutions of the discretized momentum (shallow shelf approximation; SSA) and mass conservation equations in the direction of ice flow (x). Mass conservation in the glacier is governed by

$$\frac{\partial h}{\partial t} + \frac{\partial}{\partial x}(hu) = a, \tag{1}$$

where h is the ice thickness, u is the ice velocity, and a is the surface mass balance of the glacier, which for the purposes of this study we assume is constant in space and time. We only consider the steady-state

Table 1. Parameter values for steady-state flowline simulations.

Parameter	Description	Value
a	Surface mass balance ($\mathrm{m \cdot yr^{-1}}$)	1
$\bar{A}$	Nye-Glen Law coefficient ($\mathrm{Pa^{-n} \cdot s^{-1}}$)	4.2×10^{-25}
b_x	Prograde bed slope	1×10^{-3}
C	Basal friction coefficient ($\mathrm{Pa \cdot m^{-1/n} \cdot s^{1/n}}$)	7×10^{6}
g	Acceleration due to gravity ($\mathrm{m \cdot s^{-2}}$)	9.81
m	Weertman friction law exponent	1/3
n	Nye-Glen Law exponent	3
ρ_i	Ice density ($\mathrm{kg \cdot m^{-3}}$)	917
ρ_w	Seawater density ($\mathrm{kg \cdot m^{-3}}$)	1028

case where $\frac{\partial h}{\partial t} = 0$. Conservation of momentum in the glacier is governed by

$$\frac{\partial}{\partial x}\left[2\bar{A}^{-1/n} h \left|\frac{\partial u}{\partial x}\right|^{1/n-1} \frac{\partial u}{\partial x}\right] - \theta C |u|^{m-1} u - \rho_i g h \frac{\partial}{\partial x}(h - b) = 0, \tag{2}$$

where $\bar{A}$ is the depth-averaged rate factor in Glen's flow law, n is the Glen's flow law exponent, C is the sliding law coefficient, m is the sliding law exponent, ρ_i is the density of ice, g is the acceleration due to gravity, and b is the depth of the ice sheet below sea level. The first term on the left-hand side of Equation (2) is the longitudinal stress, which plays an important role in the grounding zone under certain circumstances. The second term is basal friction, which is modified from Schoof (2007) by introducing a non-dimensional scaling factor θ (defined below). The third term is the driving stress.

The first boundary condition describes the floatation condition at the grounding line and is given by

$$\rho_i h(x = x_g) = \rho_w b(x = x_g), \tag{3}$$

where x_g is the grounding line position. This equation acts as an additional constraint on the model and is included with the mass and momentum conservation equations to ensure that the grounding line is always located at a model grid point. All model parameter values are listed in Table 1, unless otherwise specified in the text.

We model decreased basal friction in the grounding zone by prescribing idealized basal friction "ramps" as illustrated in Figure 1. We use a scaling variable θ to adjust the basal friction term of Equation (2)

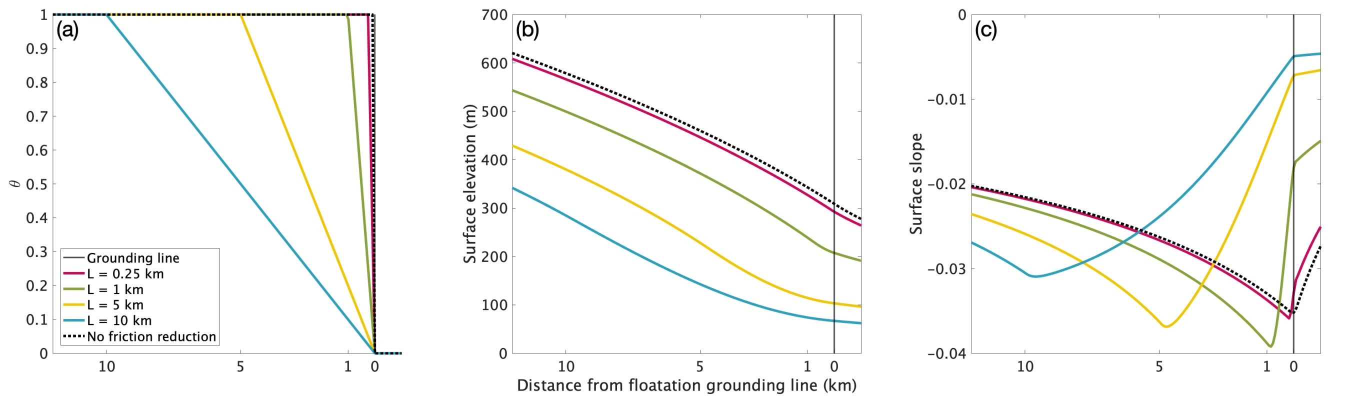

Fig. 1. (a) Basal friction ramps of varying lengths L upstream of the floatation grounding line and the control friction scenario. (b) Surface elevation profiles over basal friction ramps of varying lengths L upstream of the floatation grounding line compared to control friction scenario. (c) Same as (b), but for surface slope profiles.

such that it linearly decreases from one to zero over some distance L upstream of the grounding line until it is exactly zero at the grounding line to be consistent with the boundary condition in Equation (1). We define θ in Equation (2) to vary with x such that

$$\theta = \begin{cases} 1, & x <= x_g - L \\ \frac{x_g - x}{L}, & x_g - L < x <= x_g \\ 0, & x > x_g \end{cases} \tag{4}$$

This basal friction ramp produces an effective basal friction profile which is similar to Tsai and others (2015), but is easier to control. Physically, it can be thought of as resulting from either a transition to Coulomb sliding (as in Tsai and others, 2015) or the result of basal lubrication by seawater.

We use an iterative numerical root-finding method to solve Equations (1)-(3) simultaneously with a basal friction ramps of some specified length. These cases are compared to a control case without a basal friction ramp ($L = 0$ km). We use a numerical approach adapted from Schoof (2007), where the model grid is stretched to maintain fine horizontal grid resolution ($\Delta x\sim$ 100-200 meters, though exact grid resolution stretches with the grounding line position) just upstream of the grounding line. This numerical approach ensures that the extent of each L is well resolved and contained entirely contained within the refined grid. The flowline model is available as a public repository (Robel, 2021) and has been used and benchmarked in several previous studies (e.g., Robel and others, 2018; Christian and others, 2022; Kodama and others, 2025).

In Figure 1b, we plot the surface slope profiles for each tested friction ramp length. We find that there is a distinct surface slope profile for friction ramps of 1 km and longer as compared to a control case with no friction ramp. In the control profile, the surface slope break from a steep to shallow slope occurs at the grounding line, which by the mathematical definition of this model (Equation (2)) is the point at which ice is thin enough to float in seawater and the last contact between ice and the bed. In cases with a friction ramp, the characteristic slope break where surface slope begins to become less steep instead occurs just downstream from the point where basal friction begins to decrease. This slope break is associated with a change in the concavity of the ice surface (i.e., the second derivative of surface slope is zero), and is distinct from the transition to near constant slope that still occurs at the grounding line. The steepest surface slope is 200-300 meters downstream of the friction ramp offset in our simulations. We find that even in simulations with double and quadruple grid resolution in the grounded region (not plotted), the offset distance does not change with resolution. Thus, we conclude that this offset is capturing the longitudinal length scale associated with surface expression of basal friction.

We thus conclude from these simulations that a regime of decreasing basal friction upstream of the grounding line is accompanied by a surface slope break that is not co-located with the grounding line as defined by the floatation thickness or point of last contact with the bed. The slope breaks associated with the onset of the basal friction ramp are both larger and oriented in a different direction (steep to shallow) from the second slope breaks associated with each simulation's contact grounding line. From these results, we hypothesize that the onset of reduced basal friction upstream of the floatation/contact grounding line will be accompanied by a surface slope break which could be observable by satellite measurements of surface elevation.

Modeling Additional Potential Causes of Surface Slope Breaks

Our hypothesis from modeling connects a decreased basal friction regime to surface slope breaks displaced upstream from the floatation grounding line, but other bed properties may also have surface expression near the grounding line. We simulate the surface expressions of basal melt and changes in bed slope for comparison to our decreased basal friction scenario.

Impact of Basal Melt

To investigate the surface expression changes with basal melt upstream of the grounding line (i.e., similar to the melt from seawater intrusion modeled in Robel and others, 2022b), we experimented with the introduction of a basal melt parameter to the mass continuity equation for grounded ice (Equation (1)) such that

$$\frac{\partial h}{\partial t} + \frac{\partial (hu)}{\partial x} = a - \psi \dot{m}_i \tag{5}$$

where $\dot{m}_i$ is the rate of basal melt (melt being positive $\dot{m}_i$), and ψ is a non-dimensional scaling factor. We apply an initial basal melt rate $\dot{m}_i$ at the grounding line, then linearly decrease the basal melt rate from the floatation grounding line to zero across some distance L_m upstream of the grounding line, much like the friction ramp defined in Equation (4). We define ψ in Equation (5) to vary with x such that

$$\psi = \begin{cases} 0, & x <= x_g - L_m \\ \frac{x_g - x}{L_m}, & x_g - L_m < x <= x_g \\ 1, & x > x_g \end{cases} \tag{6}$$

We simultaneously solve Equations (2) and (5) and with $\theta = 1$, thereby removing the basal friction ramp and isolating the effect of basal melt. We tested the impact of basal melt by applying basal melting of 1 m/yr on floating ice, decreasing to zero over distances (L_m) of 1, 5, and 10 km. We found that, when the basal melt rate is 1 m/yr or lower, there is a small surface slope steepening at the onset of basal melting, as shown in Figure 2. With higher basal melt rates however, the grounding line retreats and does not achieve a steady-state, and thus our analysis is focused on 1 m/yr basal melt rates.

We conclude that, basal melting upstream of the grounding line produces a subtle surface slope break, but one that is in the direction of steepening downstream. Thus, this surface slope break has the opposite sign than the surface slope break generated by the onset of reduced basal friction, which is still by far the largest slope break even in these cases with a basal melt ramp upstream of the grounding line. In steady-state, the ice surface profile is set by a balance between the ice flux divergence and surface/basal mass balances, which remain relatively constant over most of the glacier. In the grounding zone (within a few kilometers of the grounding line), membrane stress become important and the flux divergence is higher. Thus, basal melting of just 1 m/yr under grounded ice is small comparable to this increase in flux divergence near the grounding line, and produces a relatively weak surface slope expression.

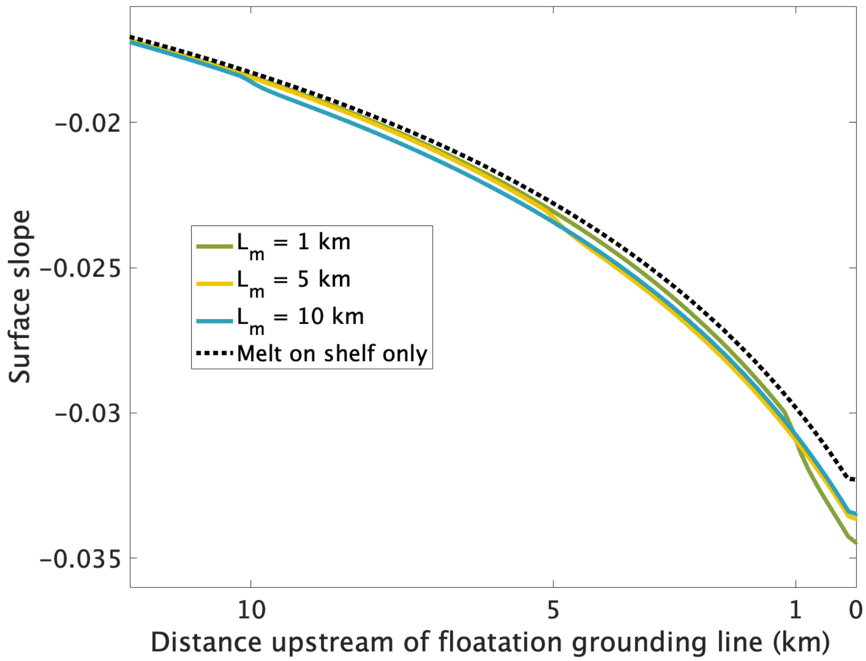

Fig. 2. Surface slope profiles over basal melt ramps of varying lengths L_m upstream of the floatation grounding line with a basal melt rate on floating ice of 1 m/yr.

It may be the case that for much higher melt rates, the associated steepening slope break would be of similar magnitude (though of opposite sign) to the shallowing slope break associated with basal friction reduction. However, we could not test such cases in the model configuration used here. Even so, basal melt under grounded ice can lubricate the bed and contribute to a decreased basal friction regime as described in our hypothesis, so the role of basal melt in the development of low-friction basal regimes should not be ignored.

Impact of a Ridge in Bed Topography

We also model the surface expression of changes to the bed slope near the grounding line to compare with the surface expression of a friction ramp and determine whether one could be confused for another. We test two bed topography regimes: first, a regime where the bed slope steepens by a factor of 2, and second, where the bed slope shoals by a factor of 4. For each bed topography considered, we model the change in surface slope occurring at lengths $L_r = 1$, 5, and 10 km upstream of the grounding line. Figure 3 visualizes the results.

When the onset of the steeper bed slope occurs 5 or 10 km upstream of the grounding line, the surface

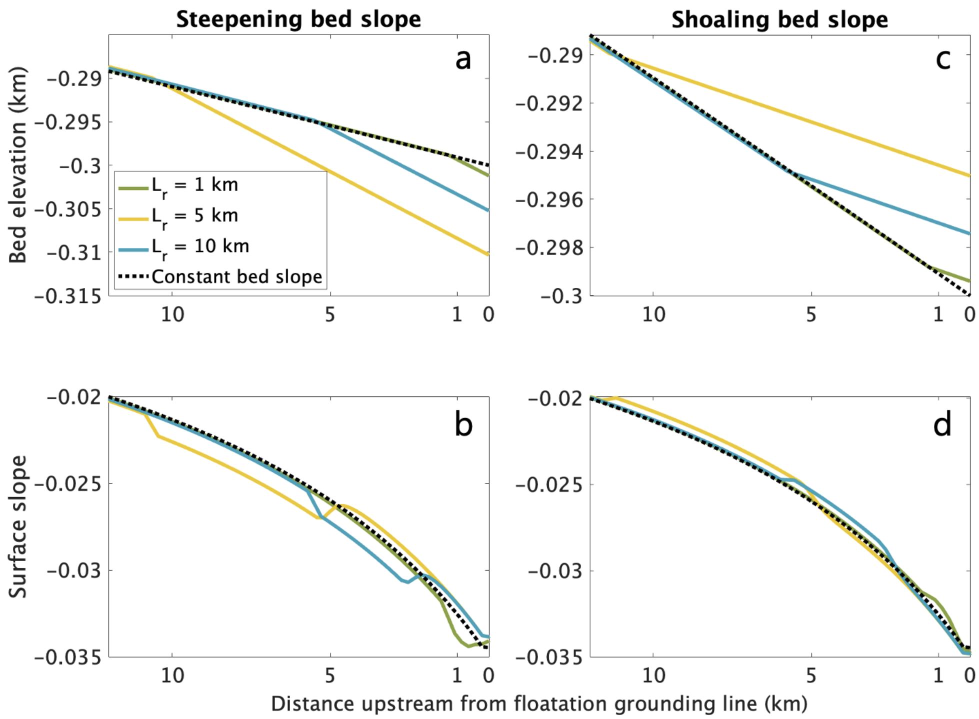

Fig. 3. Bed elevation (a,c) and surface slope (b,d) for regime of steepening (a,b) and shoaling (c,d) bed slopes at varying lengths L_r upstream of the floatation grounding line.

slope depression recovers near the grounding line, such that the break in slope caused by the steepening bed slope can be distinguished from the much greater slope break at the grounding line. However, when the onset of the steeper bed slope occurs at just 1 km upstream of the grounding line, the depression in the surface slope is sufficiently localized that it would be difficult to discern from the surface slope break at the grounding line. The surface slope minimum occurs upstream of the floatation grounding line, so a steepening bed slope near the grounding line can manifest in a surface slope break displaced upstream from the floatation grounding line. However, the change in surface slope has the opposite sign (steepening) and is considerably less than modeled for a change in basal friction.

We find that when the bed slope shoals near the grounding line, the surface slope has the opposite expression: it exhibits a minor bump at the onset of the slope change which gradually recovers. We therefore conclude that the surface expression of a shoaling bed slope near the grounding line will not be mistaken for the low basal friction regime described by the hypothesis described previously. Initial simulations with isolate bed bumps (similar to those plotted in Robel and others, 2022a, and not plotted here) produce small isolated surface expression with little resemblance to the surface expression of the friction ramp.

ANALYSIS OF ICESAT-2 DATA

The simulations above suggest a potential method for detecting regions of decreased basal friction just upstream of grounding lines using ice surface features observable from satellites. Many prior studies have used observations to constrain the grounding line position with different methods. Prior to the recent era of accurate, repeat-track altimetry with substantial coverage over Antarctica, surface slope break (denoted Point I_b hereafter) and floatation thickness were the most commonly used indicators of grounding line position (Herzfeld and others, 1994; Brunt and others, 2010). More recently, the advent of repeat-track altimetry and InSAR satellites have enabled the identification of regions of ice shelf flexure in response to tides. The inland limit of tidal flexure (denoted Point F hereafter) is a reliable indicator of the location where ice is last in contact with the bed, even if friction is low here (since tides induce detectable vertical motion of the ice surface where the ice base does not rest on the bed). Early methods for locating the grounding line () assumed that a surface slope break (Point I_b) is co-located with the last point of ice contact with the bed (Point F). Here we instead hypothesize that the surface slope break, as detected by altimetry, is the location of the onset of reduced basal friction at the bed, which may not always coincide with the last point of ice contact with the bed. We measure the extent of this "displacement" of a detectable surface slope break from the inland limit of tidal flexure using an existing datasets of these points derived from satellite altimetry.

Grounding Line Positions from ICESat-2

We leverage the dataset produced by Li and others (2022) which includes locations of grounding zone features across Antarctica derived along ICESat-2 laser altimetry repeat tracks acquired between 30 March 2019 and 30 September 2020. This dataset includes 36,765 Point I_b locations and 21,346 Point F locations selected along ICESat-2 repeat tracks. Here, we summarize their methods for estimating the locations of Point I_b and Point F.

To estimate the location of Point F, Li and others (2022) calculate temporal changes in ice elevation due to tidal influence between different repeat tracks. First, for the beam pair repeat-track data group, the elevation profiles were corrected for each individual repeat track for the across-track slope onto the nominal reference track. To find elevation anomalies, the average elevation profile over the entire dataset period was subtracted from the across-track slope-corrected elevation profile for each repeat track for the beam pair repeat-track data group. The mean absolute elevation anomaly is calculated as the average of the absolute value of all elevation anomaly profiles. Point F is picked as the point where the gradient of the mean absolute elevation anomaly first increases from zero (within error) and its second derivative reaches its positive peak.

Li and others (2022) also employed an automated method to identify estimate the location of I_b (the slope break) using only single-beam repeat-track data groups and the elevation profiles derived from them. First, they interpolated the reference elevation profile to fill in data gaps, and applied a Butterworth low-pass filter to reduce noise. To estimate the location of Point I_m, the local topographic minimum within the grounding zone, they calculated the root mean square of the reference elevation profile and identified negative peaks with values less than 0.5 m as local topographic extrema. A four-segment piecewise function was then fit to the profile, and the closest positive peak of its second derivative to a reference grounding line was used as a guide to select the potential Point I_m from local elevation minima.

Point I_b marks the location where the magnitude of the surface slope decreases most rapidly (i.e., from strongly sloped downward to flatter), identified by examining the gradient of the slope from the along-track elevation profile. Li and others (2022) calculate the absolute values of the second derivative of surface elevation and identify peaks. Point I_b is estimated as the greatest decrease in slope between the two slope break closest to the Point I_m. The chosen point I_b can occur either upstream or downstream of Point F. Since the method of Li and others (2022) selects the greatest slope break close to the grounding zone region, if this point is downstream of point F, it does not necessarily mean that a slope break does not also exist upstream of F as well. We also note that this method on selects locations where surface slope decreases the most, which should identify slope breaks similar to those we hypothesize to occur due to the onset of reduced basal friction, and not due to increased basal melt or steepening bed slope, which produce increased surface slope at the break, not decreased slope. The Li and others (2022) study provides a convenient existing dataset for identifying where prominent slope breaks exist away from F, but more locations of upstream-displaced slope breaks could be identified by reprocessing raw ICESat-2 elevation data with this goal in mind. We leave such an endeavor for future work.

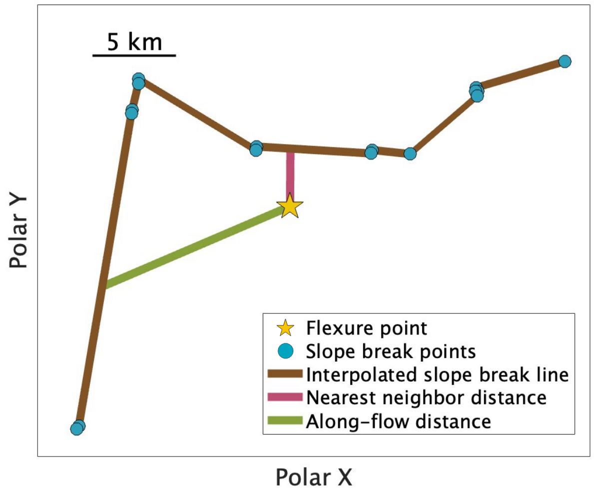

Fig. 4. Exemplar illustration of the inputs and outputs of the along-flow distance algorithm, including the flexure point (Point F) and slope break points (Point I_b) from Li and others (2022), the interpolated line of slope break points (Curve I_b), the nearest neighbor distance line, and the along-flow distance line.

Algorithm to Calculate Along-flow Displacement of Surface Slope Break

The objective of our analysis is to evaluate whether I_b points as identified by Li and others (2022) reside upstream or downstream of Point F, and then to evaluate the distance between these points. The general idea of the algorithm is that for each Point F, we construct a local curve of the I_b points within 10 km of Point F (referred to here as Curve I_b). Then, we calculate the distance between Point F and its Curve I_b along both the nearest neighbor direction and the local flow direction. Figure 4 illustrates one example of how this algorithm works.

First, we eliminate all Point I_b and Point F data lying within ice rises, as identified in the Antarctic Mapping Tool mask (Mouginot and Rignot., 2017; Rignot and others, 2013; Greene and others, 2017) to ensure small ice rises with unreliable grounding line estimates do not bias our analysis. Second, for each Point F, we find the set of I_b points within 10 km of Point F. To create Curve I_b, we linearly interpolate the points with a spacing of 10 m according to the ICESat-2 ordering as in the data provided in Li and others (2022), which is approximately radial with respect to the South Pole. In this dataset, I_b points are ordered by ICESat-2 track. While in some locations of strongly sinuous grounding line, this may lead to local interpolation error, such locations are likely to be filtered out by our quality control algorithm described further below. Third, we calculate the nearest neighbor distance between Point F and its Curve I_b for comparison to its along-flow distance. Because the data are projected onto a Antarctic polar stereographic grid, we calculate the local Euclidean distance between Point F and all points of the Curve I_b. Fourth, we calculate the along-flow distance between Point F and its Curve I_b. To determine the local flow direction from each Point F, we use the gradient of ice surface elevation determined from the MEaSUREs BedMachine product, Version 3 (Morlighem, 2022).

We assume that the surface gradient points in the flow direction (downstream). The algorithm sequentially checks whether the down-gradient direction at Point F intersects with the Curve I_b, and if not then it check whether the up-gradient direction at Point F intersects with the Curve I_b. Based on these checks Curve I_b is classified as either being downstream or upstream of Point F. If neither flow direction is found to intersect with the interpolated Curve I_b within 50 km, then no along-flow distance is reported. Finally, for those F points which have an along-flow Curve I_b, we quality control our analysis by calculating the surface gradient vector of Point I_b to determine if flowlines are strongly variable in this region. If the angle between the surface gradient vectors at Point F and the along-flow Point I_b is greater than 90 degrees, we flag this Point F-Point I_b pair as being abnormal.

Results

Of the 21,346 F points in the Li and others (2022) dataset, the algorithm found 12,807 (50.9%) with upstream displaced I_b points and 6,049 (28.3%) with downstream displaced I_b points. The algorithm was unable to identify an along-flow Point I_b for 2,430 (11.4%) F points. The remaining F points are associated with ice rises. For the upstream displaced points, the median distance across the Antarctic Ice Sheet is 1,260 m, and the mean distance is 2,019 m. For the downstream displaced points, the median distance is 1,752 m, and the mean distance is 2,394 m. When we filter the results to only include points where the difference in the surface gradient between Point F and Point I_b is less than 90 degrees (i.e., the slope break occurs along a flowline line reaching the inSAR-derived grounding line), the median and the mean distance for the upstream points is 1,085 m and 1,855 m, respectively (from 10,084 data points, or 84.8% of the total upstream displaced points). Of these upstream points with consistent surface gradients, 7,108 points (65.5%) have distances greater than the ice thickness at the Point F, indicating that the displacement may have a significant impact on ice velocity (Gudmundsson, 2003). For the downstream points, the mean and the median distance is 2,220 m and 1,540 m, respectively (from 4,634 data points, or 76.6% of the total downstream points). Figure 5 is a map plotting the 10,894 Points F where upstream Points I_b were identified and not flagged as “abnormal”.

Figure 5 includes more detailed maps of locations where ICESat-2 data indicates surface slope breaks displaced upstream from flexural grounding lines. In particular, we note particularly far upstream displacements (i.e., multiple kilometers) along the Siple Coast of the Ross Ice Shelf, the Queen Elizabeth Land portion of the Filchner-Ronne Ice Shelf and portions of Dronning Maud Land. Though there are some portions of the Amundsen Sea and Larsen C grounding lines with substantial upstream displacements, ICESat-2 tracks along the main trunks of Thwaites and Pine Island glaciers either have downstream displacements or were eliminated by the quality control algorithm, due to the strongly sinuous nature of the grounding line in this region.

This analysis connects our hypothesis from modeling with real-world observations of displacement between surface slope breaks and “true” flexural grounding lines. The prevalence of regions with such displacement around Antarctica could, with further investigation, potentially be explained by low-friction basal regimes. The implications and caveats of this work are discussed in the following section.

DISCUSSION

The central hypothesis of this study is that decreased friction upstream of grounding lines produces a significant and observable expression on the ice sheet surface in the form of a slope break displaced from the grounding line. Tsai and others (2015), in investigating the transition from power-law drag to a Coulomb regime near the grounding line, noted that such a basal friction profile tapers the ice surface slope toward the grounding line. However, that study did not further explore how to observationally determine whether such a sliding law occurs in real ice sheets. Our findings from ice surface observations demonstrate that observations support the widespread presence of such decreasing friction upstream of grounding lines at many locations around the Antarctic Ice Sheet.

The results of Tsai and others (2015) would suggest that at locations where we have identified the possibility of decreasing basal friction upstream of the grounding line, there is a stronger nonlinearity of grounding line flux. Thus, in these locations there may be greater grounding line sensitivity to climate forcing and more rapid retreat upon destabilization. Our work provides a potential method to assist with modeling efforts to determine how to interpolate basal friction conditions across and upstream of the grounding line. Seroussi and others (2014) found that different parameterizations of friction across the grounding line result in different steady state grounding line positions and retreat/advance rates, concluding

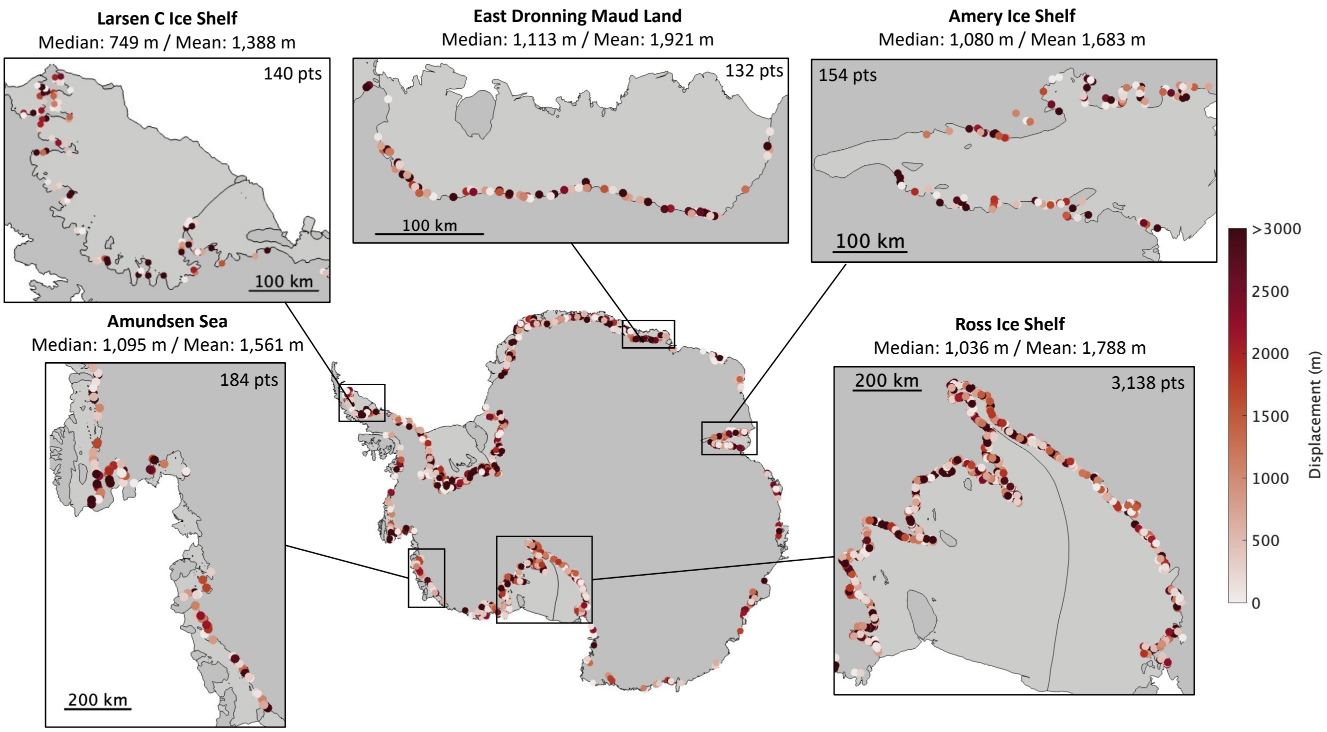

Fig. 5. A subset of F points from Li and others (2022) with upstream (up-gradient) interpolated Point I_b as identified by the along-flow distance algorithm, where the surface gradient differences between Point F and interpolated Point I_b are less than 90 degrees. F points are colored by their distance from their upstream interpolated Point I_b. Five insets highlight the findings for different regions, where the median distance, mean distance, and number of F points with upstream Point I_b are given for each region.

that sub-element parameterizations are preferable for simulating grounding line dynamics, even at low grid resolutions. Gladstone and others (2017) also find that including basal friction ramps in models upstream of grounding lines leads to improved model convergence and performance, in addition to the sort of increased sensitivity to forcing and higher retreat rates found in other studies that tested the role of friction ramps in transient marine ice sheet simulations. A recent more realistic model study of the Antarctic ice sheet response to future climate change Zhao and others (2025) indicates that smooth transitions in basal friction near Antarctic grounding line cause substantially greater future ice sheet loss due to increased flux through the grounding zone.

The displacement of the surface slope break from the grounding line has a longer history in the glaciological literature, primarily related to the discussion of "ice plains". Early geophysical studies by Jankowski and Drewry (1981) are unable to find a surface slope break near the onset of floating ice in parts of the Filchner-Ronne ice shelf and posit that the transition from floating to grounded ice is "diffuse". This presaged many later studies (Horgan and others, 2013; Christianson and others, 2016; Wilson and others, 2020) which theorized the grounding lines in many parts of Antarctica formed a more diffuse estuarine transition. With the advent of repeat-track alimetry and airborne radio echosounders, recent case studies in the Pine Island (Corr and others, 2001), Ronne-Filchner (Fricker and Padman, 2006) and Ross (Brunt and others, 2010) ice shelves have made the association between the extent of such lightly grounded "ice plain" regions and the displacement of the surface slope break from the flexure-derived grounding line position. Our results should be interpreted as consistent with prior estimates of the extents if ice plains, and providing for the first time a comprehensive mapping of such regions around Antarctica.

CONCLUSIONS

We present a method for identifying low-friction basal regimes near grounding lines of marine-terminating glaciers. Utilizing ice surface observations to constrain regions of low basal friction in ice sheet models is increasingly important to simulate the evolution of ice sheets under changing climatic conditions, especially as warm ocean water causes retreat of grounding lines around the Antarctic ice sheet. To interpret altimetry observations for the purposes of identifying low-friction basal regimes, we suggest that future efforts be dedicated to re-processing raw ICESat-2 tracks to identify the closest true slope break to the hydrostatic grounding line. Data assimilation methods constrained by observations of bed topography, ice sheet surface elevation, and ice surface velocity can also be leveraged to directly constrain basal friction and melt near grounding lines while controlling for the potential influence of bed topography. Our study shows that current observational datasets likely provide models with sufficiently strong constraints to more confidently construct realistic basal friction parameterizations in the critical region upstream of the grounding line.

OPEN RESEARCH SECTION

All code used to run models, analyze data and generate figures in this study is publicly available at the following GitHub repository: https://github.com/aarobel/Surface-Expression-Of-Low-Basal-Friction. This repository also includes a pre-processed dataset (ICESat2_Li2022_frictionramplength.csv) listing the locations of grounding line points with upstream displaced surface slope breaks.

ACKNOWLEDGEMENTS

Thank you to Danielle Grau, Madeline Mamer, and Crispin Gambill for their valuable input during the completion of this work. The authors were supported by Startup funding from the Georgia Tech Research Corporation.

REFERENCES

Brondex J, Gagliardini O, Gillet-Chaulet F and Durand G (2017) Sensitivity of grounding line dynamics to the choice of the friction law. *Journal of Glaciology*, **63**(241), 854–866

Brunt KM, Fricker HA, Padman L, Scambos TA and O'Neel S (2010) Mapping the grounding zone of the Ross Ice Shelf, Antarctica, using ICESat laser altimetry. *Annals of Glaciology*, **51**(55), 71–79

Christian JE, Robel AA and Catania G (2022) A probabilistic framework for quantifying the role of anthropogenic climate change in marine-terminating glacier retreats. *The Cryosphere*, **16**(7), 2725–2743

Christianson K, Jacobel RW, Horgan HJ, Alley RB, Anandakrishnan S, Holland DM and DallaSanta KJ (2016) Basal conditions at the grounding zone of Whillans Ice Stream, West Antarctica, from ice-penetrating radar. *Journal of Geophysical Research: Earth Surface*, **121**(11), 1954–1983

Corr HF, Doake C, Jenkins A and Vaughan DG (2001) Investigations of an "ice plain" in the mouth of Pine Island Glacier, Antarctica. *Journal of Glaciology*, **47**(156), 51–57

Fricker HA and Padman L (2006) Ice shelf grounding zone structure from icesat laser altimetry. *Geophysical Research Letters*, **33**(15)

Gadi R, Rignot E and Menemenlis D (2023) Modeling ice melt rates from seawater intrusions in the grounding zone of Petermann Gletscher, Greenland. *Geophysical Research Letters*, **50**(24), e2023GL105869

Gladstone RM, Warner RC, Galton-Fenzi BK, Gagliardini O, Zwinger T and Greve R (2017) Marine ice sheet model performance depends on basal sliding physics and sub-shelf melting. *The Cryosphere*, **11**(1), 319–329

Greene CA, Gwyther DE and Blankenship DD (2017) Antarctic mapping tools for MATLAB. *Computers & Geosciences*, **104**, 151–157

Gudmundsson GH (2003) Transmission of basal variability to a glacier surface. *Journal of Geophysical Research: Solid Earth*, **108**(B5)

Herzfeld UC, Lingle CS and Lee LH (1994) Recent advance of the grounding line of Lambert Glacier, Antarctica, deduced from satellite-radar altimetry. *Annals of Glaciology*, **20**, 43–47

Horgan HJ, Alley RB, Christianson K, Jacobel RW, Anandakrishnan S, Muto A, Beem LH and Siegfried MR (2013) Estuaries beneath ice sheets. *Geology*, **41**(11), 1159–1162

Jankowski EJ and Drewry D (1981) The structure of west antarctica from geophysical studies. *Nature*, **291**(5810), 17–21

Kodama ST, Pico T, Robel AA, Christian JE, Gomez N, Vigilia C, Powell E, Gagliardi J, Tulaczyk S and Blackburn T (2025) Impact of glacial isostatic adjustment on zones of potential grounding line persistence in the ross sea embayment (antarctica) since the last glacial maximum. *The Cryosphere*, **19**(8), 2935–2948

Li T, Dawson GJ, Chuter SJ and Bamber JL (2022) A high-resolution Antarctic grounding zone product from ICESat-2 laser altimetry. *Earth System Science Data*, **14**(2), 535–557

Morlighem M (2022) MEaSUREs BedMachine Antarctica, Version 3 (doi: 10.5067/FPSU0V1MWUB6)

Mouginot BS J and Rignot E (2017) MEaSUREs Antarctic Boundaries for IPY 2007-2009 from Satellite Radar, Version 2 (doi: 10.5067/AXE4121732AD)

Rignot E, Jacobs S, Mouginot J and Scheuchl B (2013) Ice-Shelf Melting Around Antarctica. *Science*, **341**(6143), 266–270 (doi: 10.1126/science.1235798)

Rignot E, Ciracì E, Scheuchl B, Tolpekin V, Wollersheim M and Dow C (2024) Widespread seawater intrusions beneath the grounded ice of Thwaites Glacier, West Antarctica. *Proceedings of the National Academy of Sciences*, **121**(22), e2404766121

Robel A (2021) aarobel/ssasimplem: Release of ssasimplem for publication (doi: 10.5281/zenodo.5245271)

Robel AA, Roe GH and Haseloff M (2018) Response of marine-terminating glaciers to forcing: time scales, sensitivities, instabilities, and stochastic dynamics. *Journal of Geophysical Research: Earth Surface*, **123**(9), 2205–2227

Robel AA, Pegler SS, Catania G, Felikson D and Simkins LM (2022a) Ambiguous stability of glaciers at bed peaks. *Journal of Glaciology*, **68**(272), 1177–1184

Robel AA, Wilson E and Seroussi H (2022b) Layered seawater intrusion and melt under grounded ice. *The Cryosphere*, **16**, 451–469 (doi: 10.5194/tc-16-451-2022)

Schoof C (2007) Ice sheet grounding line dynamics: Steady states, stability, and hysteresis. *Journal of Geophysical Research*, **112**, F03S28 (doi: 10.1029/2006JF000664)

Seroussi H, Morlighem M, Larour E, Rignot E and Khazendar A (2014) Hydrostatic grounding line parameterization in ice sheet models. *The Cryosphere*, **8**(6), 2075–2087

Seroussi H, Nowicki S, Simon E, Abe-Ouchi A, Albrecht T, Brondex J, Cornford S, Dumas C, Gillet-Chaulet F, Goelzer H and others (2019) initMIP-Antarctica: an ice sheet model initialization experiment of ISMIP6. *The Cryosphere*, **13**(5), 1441–1471

Tsai VC, Stewart AL and Thompson AF (2015) Marine ice-sheet profiles and stability under coulomb basal conditions. *Journal of Glaciology*, **61**(226), 205–215 (doi: 10.3189/2015JoG14J221)

Wilson EA, Wells AJ, Hewitt IJ and Cenedese C (2020) The dynamics of a subglacial salt wedge. *Journal of Fluid Mechanics*, **895**, A20

Zhao C, Gladstone R, Zwinger T, Gillet-Chaulet F, Wang Y, Caillet J, Mathiot P, Saraste L, Jager E, Galton-Fenzi BK and others (2025) Subglacial water amplifies Antarctic contributions to sea-level rise. *Nature Communications*, **16**(1), 3187


(a)
θ
Grounding line
L = 0.25 km
L = 1 km
L = 5 km
L = 10 km
No friction reduction
(b)
Surface elevation (m)
(c)
Surface slope
Distance from floatation grounding line (km)

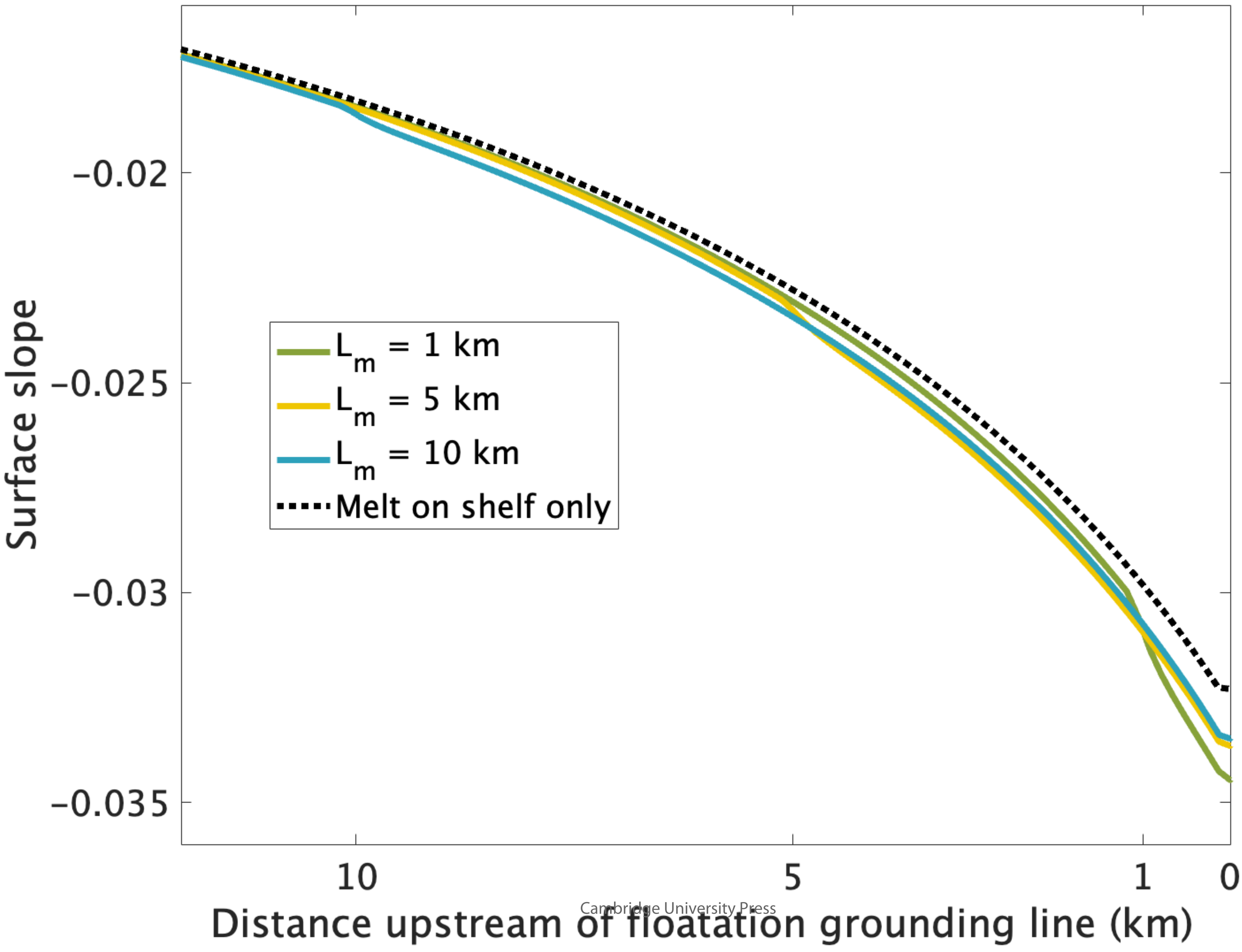
Surface slope
−0.02
−0.025
−0.03
−0.035
L_m = 1 km
L_m = 5 km
L_m = 10 km
Melt on shelf only
10
5
1
0
Distance upstream of floatation grounding line (km)

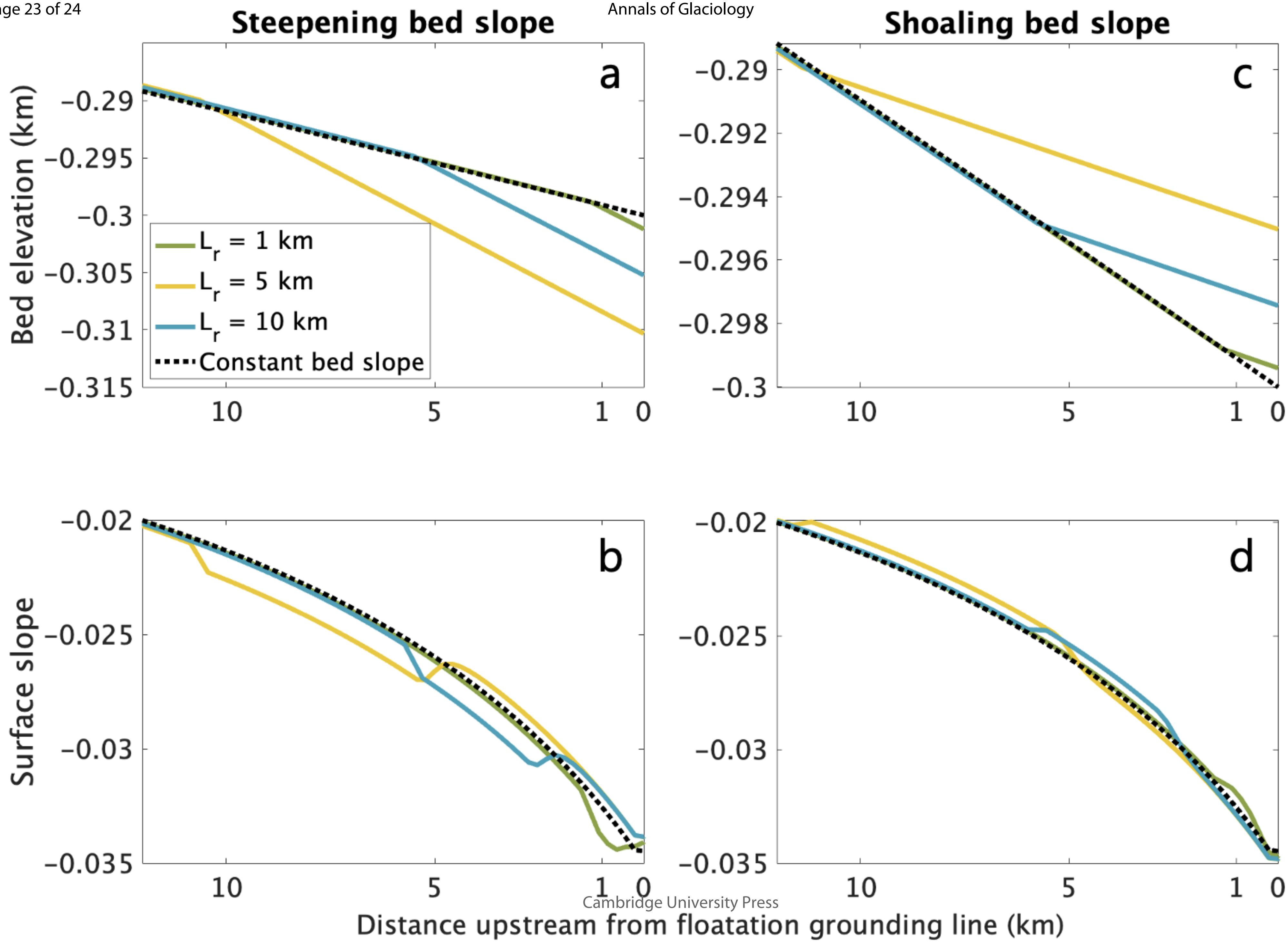
Steepening bed slope
Shoaling bed slope
a
b
c
d
Bed elevation (km)
Surface slope
L_r = 1 km
L_r = 5 km
L_r = 10 km
Constant bed slope
Distance upstream from floatation grounding line (km)

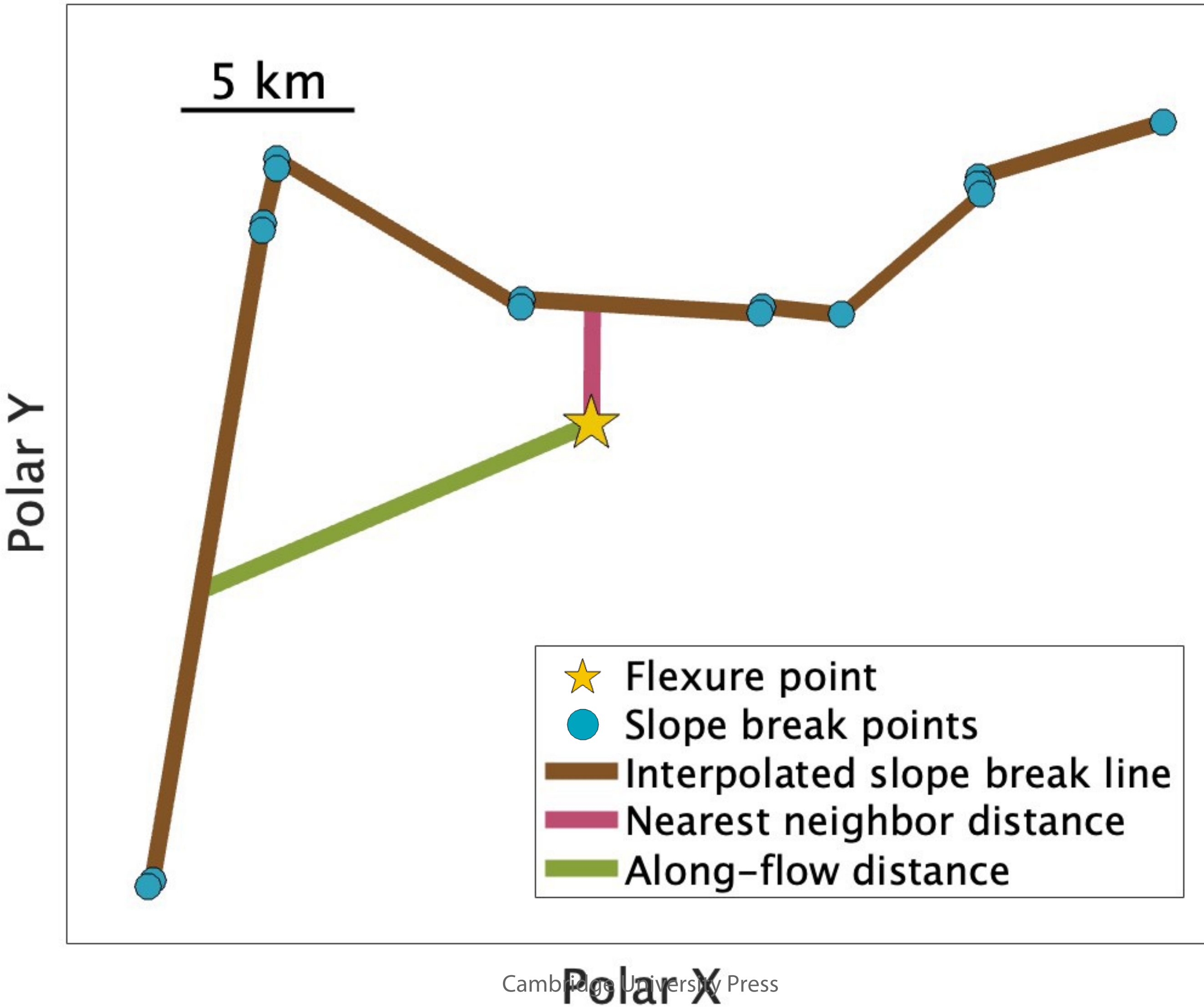
5 km
Polar Y
Polar X
Flexure point
Slope break points
Interpolated slope break line
Nearest neighbor distance
Along-flow distance

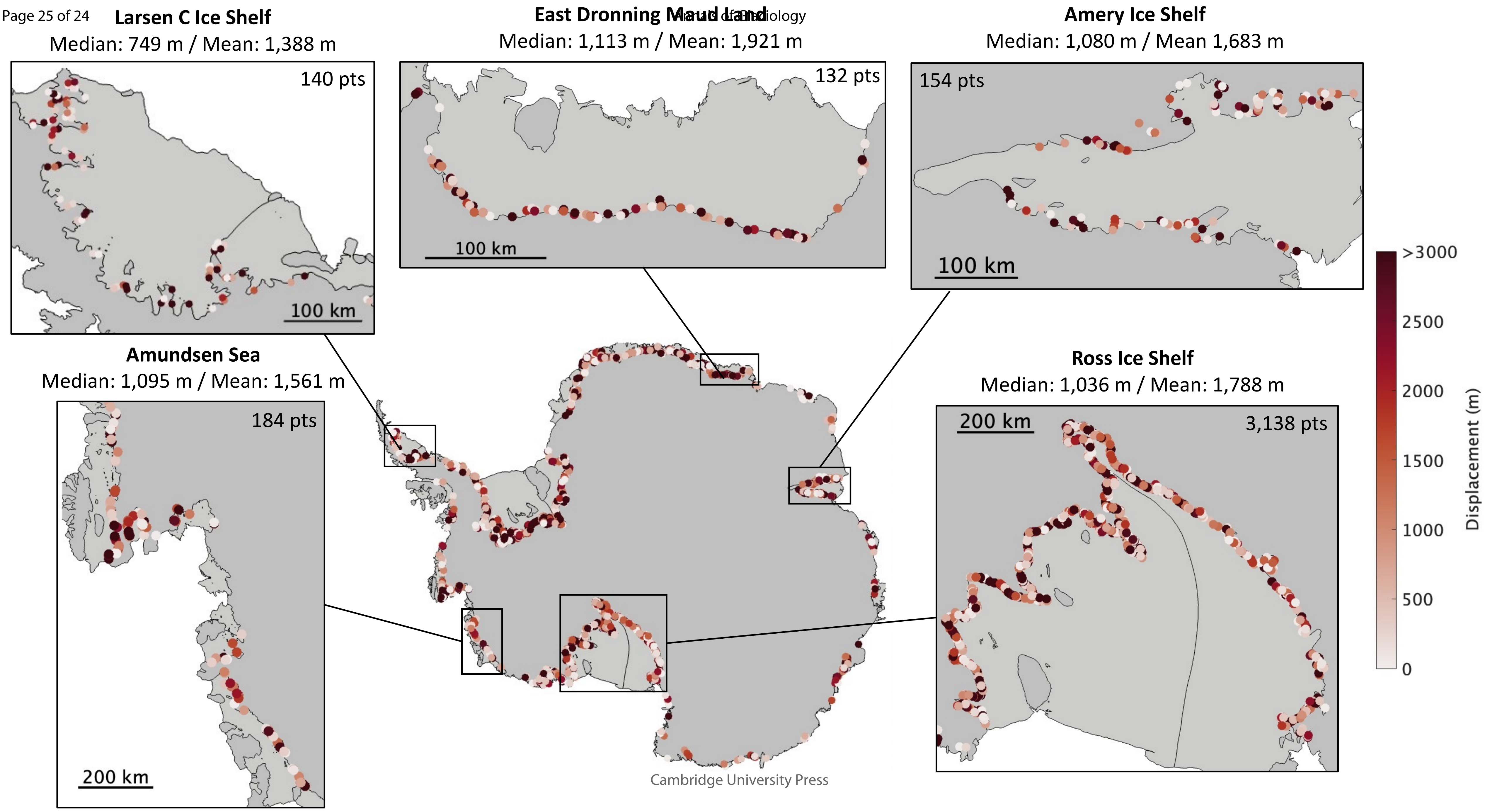
Larsen C Ice Shelf
Median: 749 m / Mean: 1,388 m
140 pts
100 km
East Dronning Maud Land
Median: 1,113 m / Mean: 1,921 m
132 pts
100 km
Amery Ice Shelf
Median: 1,080 m / Mean 1,683 m
154 pts
100 km
Amundsen Sea
Median: 1,095 m / Mean: 1,561 m
184 pts
200 km
Ross Ice Shelf
Median: 1,036 m / Mean: 1,788 m
200 km
3,138 pts
>3000
2500
2000
1500
1000
500
0
Displacement (m)